3. RESULTS

3.1 GM-CSF- and GM-CSF/IL-3-Deficient Mice Develop Autoimmune Diseases

Earlier work in our laboratory delineated a PAP-like disease in GM-CSF- and GM-CSF/IL-3-deficient mice (36, 55). GM-CSF/IL-3-deficient mice also showed a weaker contact hypersensitivity reaction and an increased number of circulating eosinophils (55). Pathological analysis of aged mutant animals (older than 8 months) on the C57Bl/6, but not on the Balb/c background, unexpectedly revealed additional disorders. Aged GM-CSF- and GM-CSF/IL-3-deficient mice developed an immune-mediated glomerulonephritis with B and T cell aggregates in the renal pelvis (Figure 3.1.1 A and B). Similar findings were obtained in 22/22 GM-CSF- and 17/17 GM-CSF/IL-3-deficient mice. Consistent with these lesions, a significant proportion of GM-CSF- and GM-CSF/IL-3-deficient mice generated: anti-dsDNA autoantibodies, anti-C1q-reactivity, and rheumatoid factors (Figure 3.1.1 C and D). The renal pathology, together with the set of autoantibodies, characterized a SLE-like disorder in these animals (8, 89). No significant differences in the occurrence of autoimmune diseases between male and female GM-CSF- or GM-CSF/IL-3-deficient mice could be found (11 of the GM-CSF-deficient and 8 of the GM-CSF/IL-3-deficient mice that developed the disease, were males).

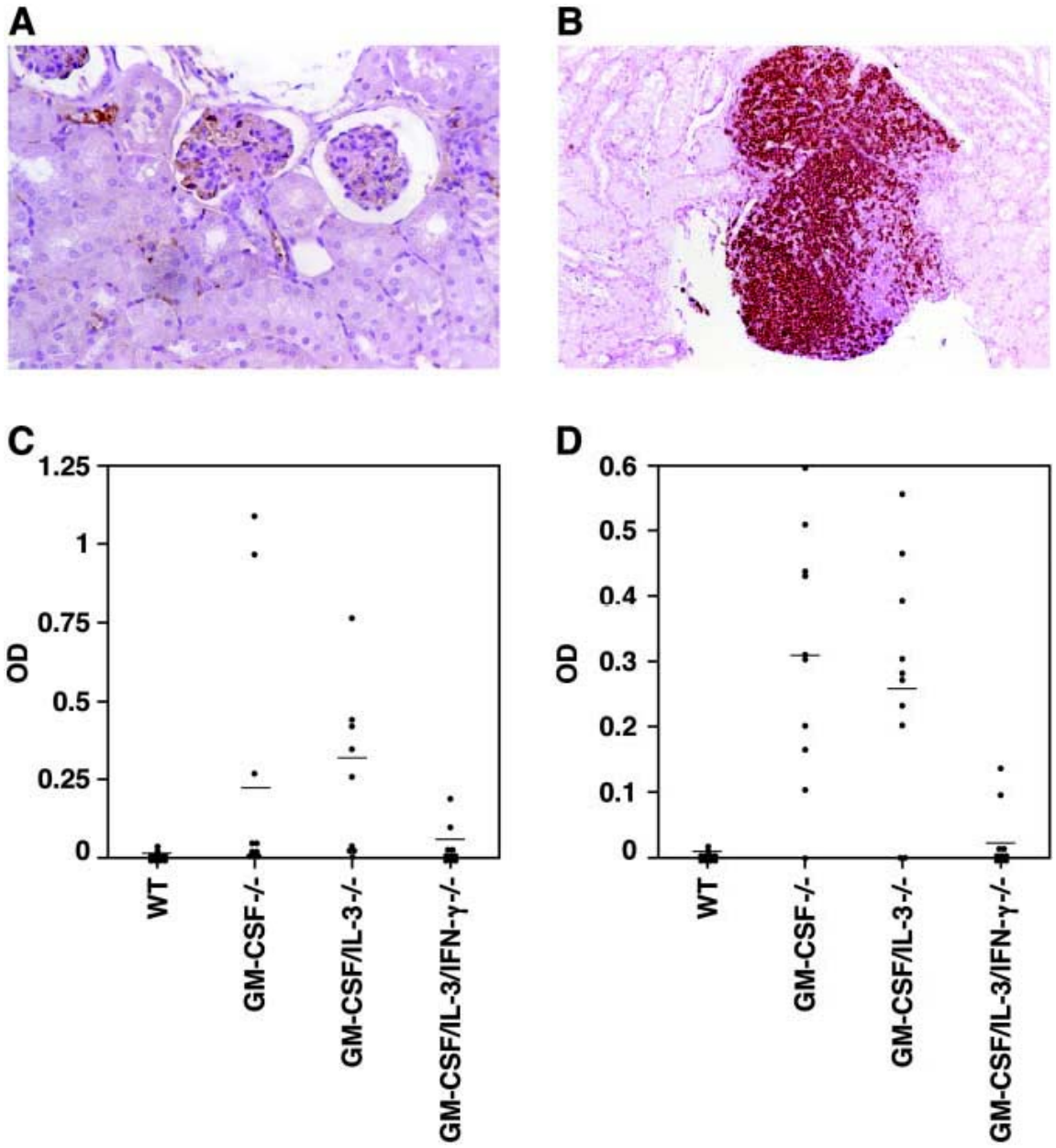

Figure 3.1.1 Aged GM-CSF- and GM-CSF/IL-3-deficient mice developed a SLE-like disorder. (A) Membrano-proliferative glomerulonephritis with Ig deposition in a GM-CSF-deficient mouse, anti-κ antibody (original magnification x 400). (B) $B220^{+}$ B cell aggregates in the renal pelvis of a GM-CSF-deficient mouse (original magnification x 400). (C) Anti-dsDNA autoantibodies. (D) Anti-C1q reactivity.

The mechanisms underlying autoimmune diseases in several murine models involve the impaired phagocytosis of apoptotic cells (95). To test whether GM-CSF/IL-3 deficiency results in a similar defect, I injected dexamethasone-induced apoptotic thymocytes into the peritoneal cavities of WT and GM-CSF/IL-3-deficient mice and measured the phagocytic activity of their resident macrophages (126). Cytospins of peritoneal washings disclosed a marked reduction in the uptake of apoptotic bodies by macrophages from mutant mice compared with WT animals (Figure 3.1.2 A and B) (8). Similar defects were also present in GM-CSF-deficient mice (5/5 animals affected). Moreover, fluorescent labeling of apoptotic thymocytes with 5[6]-TAMRA, SE, prior to injection, revealed that fewer than one-third of the Mac-1 positive cells from GM-CSF/IL-3-deficient mice were associated with apoptotic material, in contrast to more than three-quarters of the Mac-1 positive cells from the control animals (Figure 3.1.2 C and D) (8). This compromised phagocytosis of apoptotic cells is consistent with earlier work showing the defective uptake of: pulmonary surfactant, bacteria, and latex beads by alveolar macrophages from GM-CSF-deficient mice (41).

Whereas all mutant mice analyzed showed an impaired phagocytosis of apoptotic cells, the variable titers of anti-dsDNA autoantibodies indicate that additional factors may also contribute to disease severity.

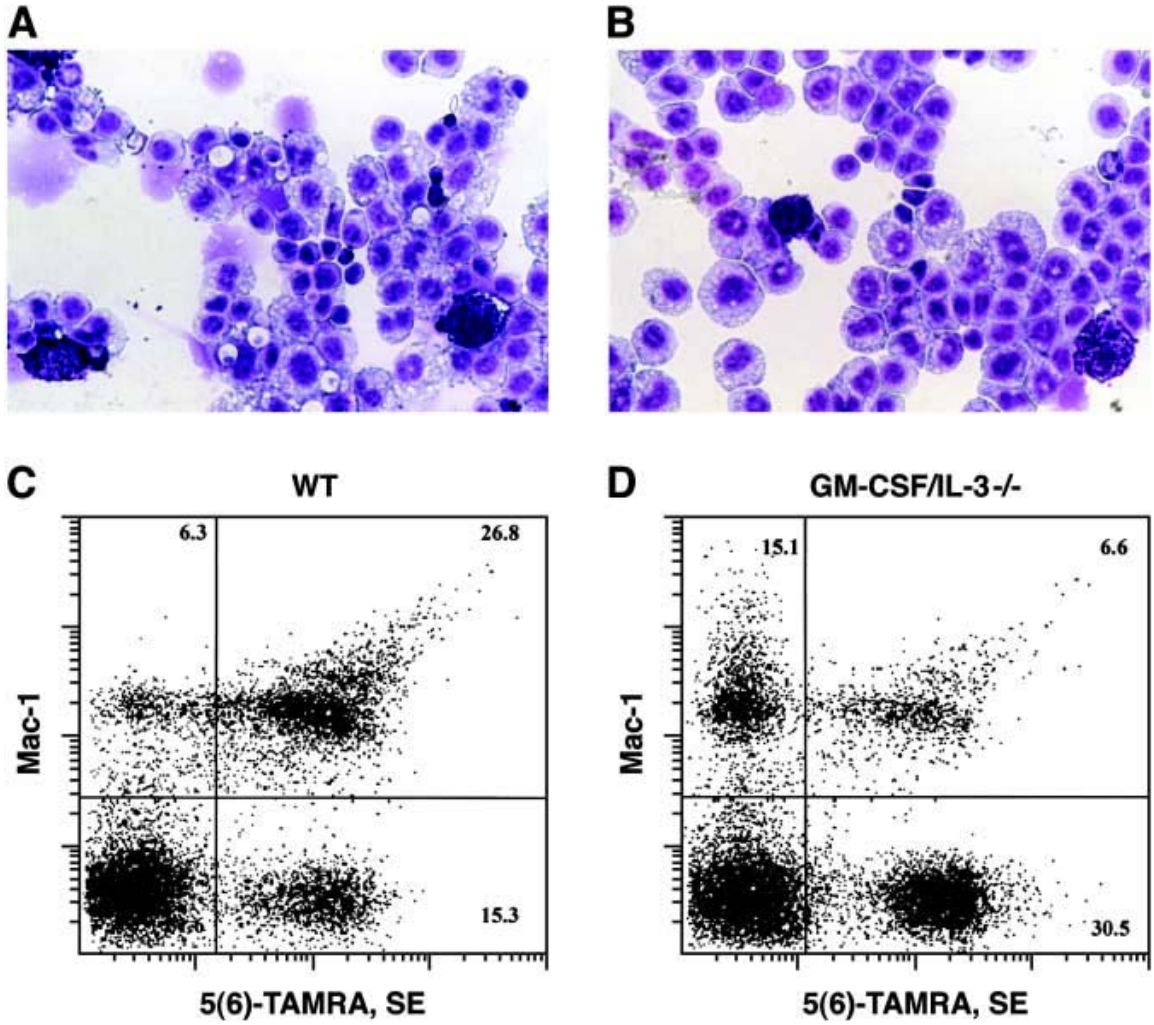

Figure 3.1.2 Impaired phagocytosis of apoptotic cells in GM-CSF- and GM-CSF/IL-3-deficient mice. Dexamethasone-induced apoptotic thymocytes, derived from GM-CSF-deficient mice, were injected into the peritoneal cavities of WT or GM-CSF/IL-3-deficient mice. (A and B) Stained cytospins of harvested cells from: (A) WT mouse (original magnification x 400) and (B) GM-CSF/IL-3-deficient mouse (original magnification x 400). Similar results were obtained from 5 independent experiments, and GM-CSF-deficient mice manifested comparable defects. (C and D) Apoptotic thymocytes were labeled with 5[6]-TAMRA, SE, before injection, and FACS® was used to analyze the harvested peritoneal cells: (C) WT mouse, (D) GM-CSF/IL-3-deficient mouse. Results were representative from 6 independent experiments.

We then wondered whether other organs in these mice would manifest signs of autoimmunity. Surprisingly, histological analysis of most of the pancreases of the aged GM-CSF/IL-3 doubly deficient mice on the C57Bl/6 background revealed pathological pancreatic islets, infiltrated with $B220^+$ B and $CD3^+$ T cells, consistent with insulitis (Figure 3.1.3 A and B). The total number of pancreatic islets in the affected animals was markedly reduced (~30%, preliminary data). In contrast, GM-CSF singly deficient mice did not show infiltrated pancreatic islets, but most of these mice manifested signs of a peri-insulitis ($B220^+$, $CD3^+$). No pancreatic infiltrates could be found in IL-3-, IFN-γ-, or GM-CSF/IL-3/IFN-γ-deficient mice on the C57Bl/6 and in GM-CSF-, IL-3- and GM-CSF/IL-3-deficient mice on the Balb/c background. Accordingly, FBS measurements showed elevated sugars with 22 out of 30 GM-CSF/IL-3-deficient mice at the age of 8 months ($P < 0.0001$, versus WT) (Figure 3.1.3 C). Further, glucose tolerance tests with a cohort of the GM-CSF/IL-3-deficient mice revealed 9 out of 12 mice with pathological glucose tolerance profiles ($P = 0.00008$, versus WT) (Figure 3.1.3 D). In all the cases tested, the pathological glucose tolerance profiles went in parallel with elevated measurements of FBS. The insulitis, together with the elevated levels of FBSs, are both characteristic for autoimmune diabetes (89, 133). In contrast, pathological FBSs could not be found in WT, GM-CSF-, IL-3-, IFN-γ-, or GM-CSF/IL-3/IFN-γ-deficient mice on the C57Bl/6 background nor in the cytokine-deficient mice on the Balb/c background (Figure 3.1.3 C). Glucose tolerance test in all these mice were normal except that one out of 6 GM-CSF/IL-3/IFN-γ-deficient mice showed a pathological glucose tolerance profile suggesting a latent diabetes in this mouse (Figure 3.1.3 E).

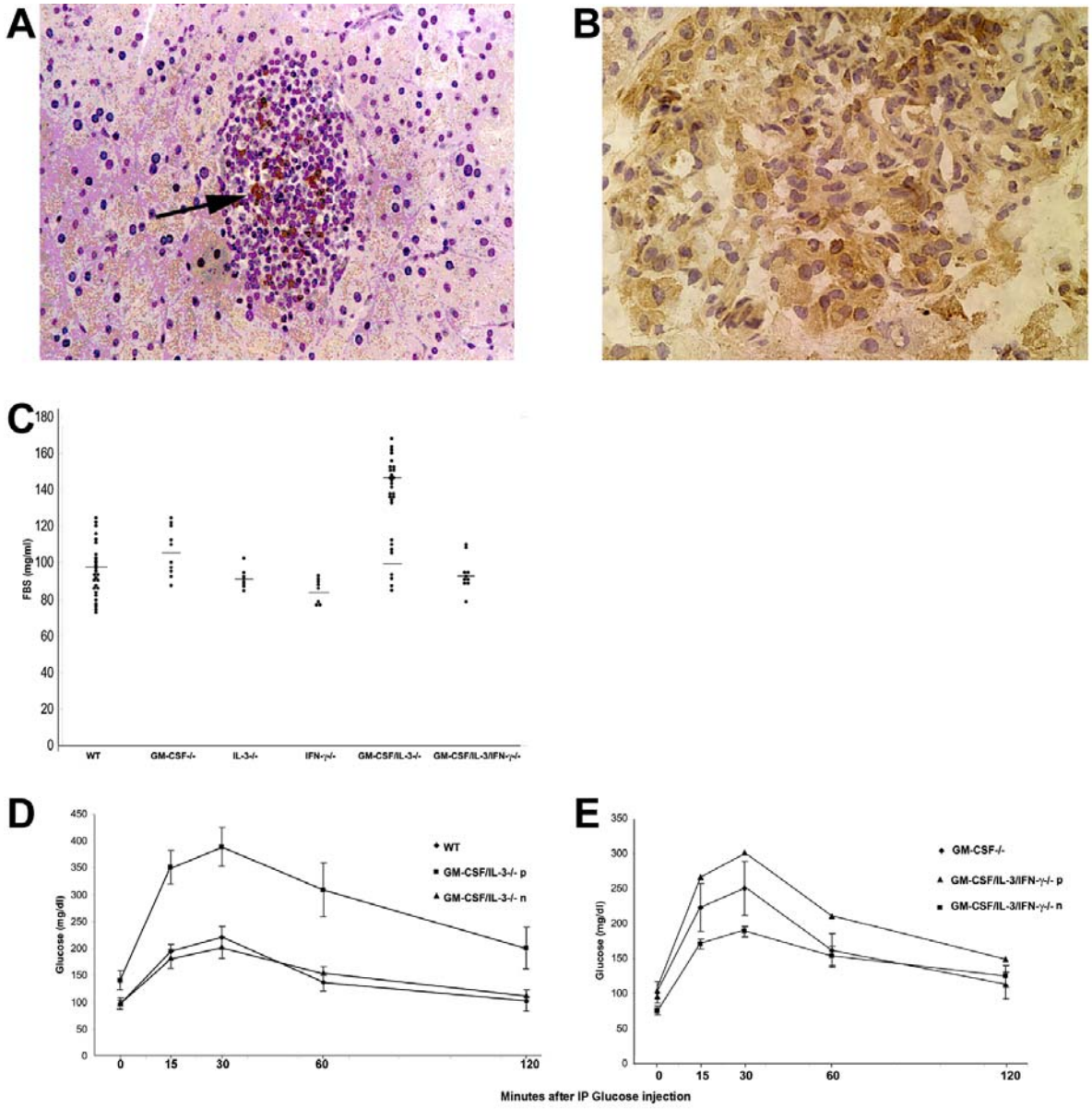

Figure 3.1.3 Aged GM-CSF/IL-3-deficient mice developed an autoimmune diabetes. (A and B) Pancreatic islet of an aged GM-CSF/IL-3-deficient mouse infiltrated with: (A) $B220^+$ B cells (original magnification x 400), and (B) with $CD3^+$ T cells (HRP-labeled anti-$CD3^+$, original magnification x 600). (C) FBS measurements of 8-months-old: WT (n = 30), GM-CSF- (n = 10), IL-3- (n = 8), IFN-γ- (n = 8), GM-CSF/IL-3- (n = 30), and GM-CSF/IL-3/IFN-γ-deficient mice (n = 10). Whereas 22 out of 30 GM-CSF/IL-3-deficient mice clearly showed a pathologically elevated FBS, no diabetes could be

observed in: WT, GM-CSF-, IL-3-, IFN-γ-, and GM-CSF/IL-3/IFN-γ-deficient mice. (D and E) Glucose tolerance tests were performed after administration of 3g/kg body weight glucose solution. Blood sugars were measured at times: 0, 15, 30, 60, and 120 min. Normal (n) glucose tolerance profiles showed: WT (n = 8), GM-CSF- (n = 6), and IL-3-deficient (n = 6; not shown) mice. Pathological (p) profiles showed: 9 out of 12 GM-CSF/IL-3- and one out of 6 GM-CSF/IL-3/IFN-γ-deficient mice.

The thymi of GM-CSF/IL-3-deficient mice maintained normal T cell maturation and normal T cell numbers as measured by FACS®. FACS® analysis of the spleens of diabetic versus WT mice revealed no significant differences in total numbers of: CD3ε, CD4, CD8, I-A^b, Mac-1, Gr-1, NK1.1, NK1.1-T, CD11c, CD80, CD86, and B220 positive cells.

Insulin-Dependent Diabetes Mellitus (IDDM), or autoimmune diabetes, is a highly regulated disease (134, 135). Three major phases of the disease can be distinguished: firstly, the generation of T lymphocytes reactive to proteins made by pancreatic islet β cells, secondly, the infiltration of these cells and other leukocytes into the islets, and thirdly, the terminal destruction of β cells leading to hyperglycemia (130). The NOD mouse has been instrumental in defining these three phases of disease, but they are even more clear in the NOD BDC2.5 TCR transgenic model of diabetes (136). BDC2.5 TCR transgenic mice carry the rearranged TCR from a diabetogenic T cell clone isolated from a NOD mouse (137). Autoreactive cells of BDC2.5 mice on the NOD genetic background begin to infiltrate the pancreatic islets 2 weeks after birth, but do not develop diabetes until several months later (136). The research groups of Diane Mathis and Jim Allison could demonstrate that CTLA-4 was involved in the development of diabetes in these mice (130). Injection of an anti-CTLA-4 monoclonal antibody (mAb) into young BDC2.5 transgenic mice led to a rapid development of diabetes, months before these mice would normally become diabetic (130). Surprisingly, this effect was only observed when the anti-CTLA-4 mAb was injected during a narrow time window, namely before the initiation of an insulitis (130).

There is now growing evidence that DCs, in combination with $CD25^+$ $CD4^+$ regulatory T cells, play an important role in preventing autoimmune diseases (138, 139). Our group previously described a defect in DC function of GM-CSF/IL-3-deficient mice, whereas total numbers of DCs were found in the normal range (55). I could not identify any significant differences in the total cell numbers between DCs or regulatory $CD25^+$ $CD4^+$ T cells of diabetic GM-CSF/IL-3-deficient and non-diabetic WT mice by FACS® analysis (6 mice investigated in each group).

Since in autoimmune diabetes the insulin-producing β cells of the pancreatic islets are destroyed by T lymphocyte-provoked mechanisms (135), and since treatment with an anti-CTLA-4 mAb of a transgenic mouse model on the NOD background rapidly provoked diabetes (130), I decided to test whether I could induce diabetes in the young GM-CSF/IL-3-deficient mice, by treating them with this anti-CTLA-4 mAb. Indeed, treatment of the young GM-CSF/IL-3-deficient mice on the C57Bl/6 background (n = 30) with 100 µg of anti-CTLA-4 mAb at the ages of: 12, 15, and 18 days, provoked the onset of diabetes in > 70% of these animals within 3 weeks after the first injection ($P < 0.0001$, versus WT) (Figure 3.1.4).

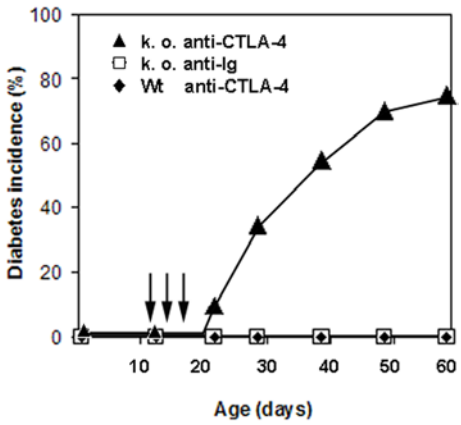

Figure 3.1.4 Time course of diabetic development in GM-CSF/IL-3-deficient mice (k. o.) after anti-CTLA-4 mAb treatment. Intraperitoneal injection of GM-CSF/IL-3-deficient and WT mice with 3 x 100 µg of anti-CTLA-4 mAb (arrows) provoked the onset of diabetes in > 70% of the cytokine-deficient mice within 3 weeks after the first injection

(*n* = 30 GM-CSF/IL-3-deficient mice). No diabetes could be induced in the GM-CSF/IL-3-deficient mice with an isotype-matched IgG control antibody (*n* = 15 mice) or in WT mice treated with anti-CTLA-4 mAb (*n* = 25).

The diagnosis of autoimmune diabetes in the anti-CTLA-4 mAb treated GM-CSF/IL-3-deficient mice was confirmed by elevated FBSs (Figure 3.1.5 A), and histologically. All the mice with elevated FBSs showed inflammatory infiltrates in their pancreatic islets, consistent with insulitis (Figure 3.1.5 B and C). Mice without elevated FBS, generally, did not reveal lymphocytic infiltrates. FACS® analysis of mice with induced diabetes did not show any differences in total numbers of DCs or regulatory $CD25^+$ $CD4^+$ T cells, compared to non-diabetic controls (3 mice tested in each group).

Similar to the findings in BDC2.5 transgenic NOD mice, the time frame of the anti-CTLA-4 mAb injection was relevant (130). Initiating anti-CTLA-4 treatment at the age of 3 weeks or older had no effect on the development of diabetes (i. e. a time course of onset of diabetes in these mice did not differ from the untreated controls) (data from 6 GM-CSF/IL-3-deficient mice).

Despite the occurrence of autoimmune diseases, GM-CSF- and GM-CSF/IL-3-deficient mice failed to manifest an increase in spontaneous tumor formation over 14 months of observation.

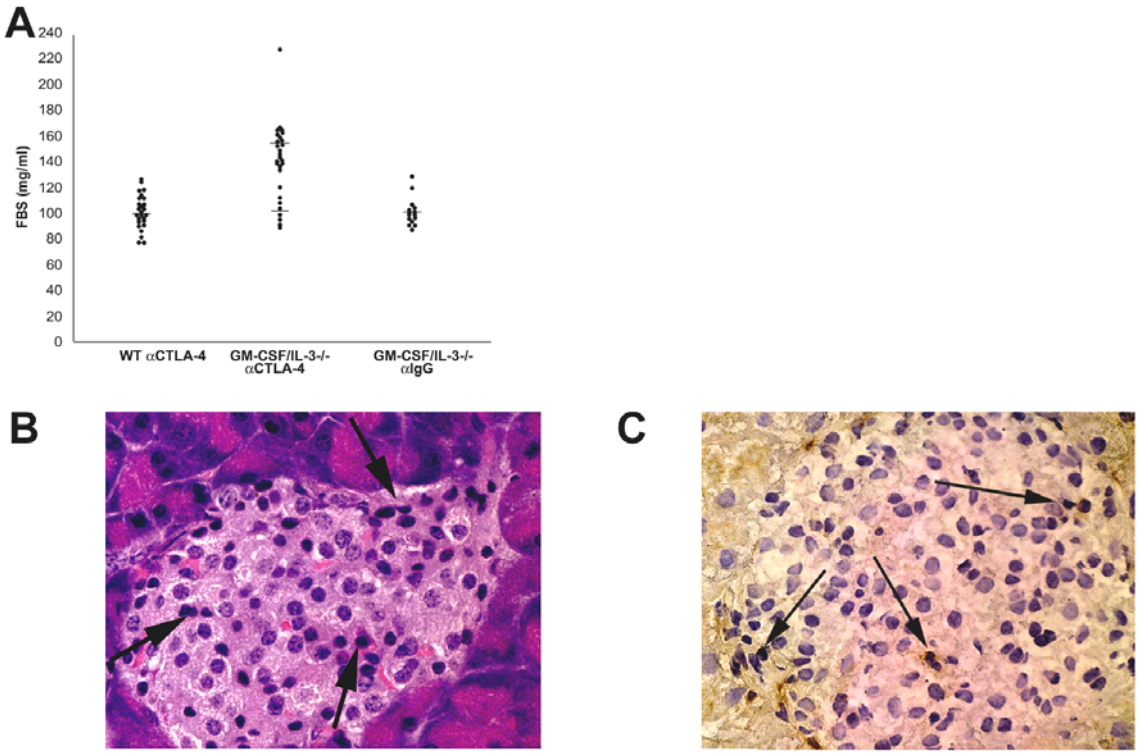

Figure 3.1.5 Anti-CTLA-4 mAb (αCTLA-4) treatment induced an autoimmune diabetes in GM-CSF/IL-3-deficient mice. (A) FBS measurements, performed 30 days after the first injection of anti-CTLA-4 mAb, showed pathologically elevated FBS in 22 out of 30 anti-CTLA-4-treated mice ($P < 0.0001$, versus WT). No diabetes induction could be observed with treatment of GM-CSF/IL-3-deficient mice with an IgG isotype-matched control Ab ($n = 15$ mice) or with anti-CTLA-4 treatment of WT mice ($n = 25$) ($P < 0.0001$, versus diabetic anti-CTLA-4 treated GM-CSF/IL-3-deficient mice). (B and C) Pancreatic islet of an anti-CTLA-4 treated GM-CSF/IL-3-deficient mouse revealing (B) inflammatory infiltrates (arrows, H & E stain, original magnification x 400), and (C) the cell type of the inflammatory cells as T cells (arrows, anti-$CD8^+$ stain, original magnification x 400).

3.2 GM-CSF/IFN-γ- and GM-CSF/IL-3/IFN-γ-Deficient Mice Often Develop Lethal Infections

As IFN-γ-deficient mice display an enhanced susceptibility to chemical carcinogenesis (19, 114, 119), we wished to test whether GM-CSF and IL-3 cooperate in tumor suppression. To answer this question, we generated GM-CSF/IFN-γ- and GM-CSF/IL-3/IFN-γ-deficient mice. Surprisingly, this compound knock out mice demonstrated reduced survival compared to the parental strains (Figure 3.2.1 A) (8). Whereas the litter sizes were nearly normal, ~40% of the newborn animals succumbed to overwhelming pneumonia within the first few weeks of life (Figure 3.2.1 B). Lung washings with 0.9% NaCl solution consistently grew *Pasteurella pneumotropica*, a gram-negative coccobacillus that normally colonizes the oropharynx of rodents without causing disease (140). Lethal infections in the mutant animals likely reflected, at least in part, diminished bacterial ingestion and killing. In this regard, 4 out of 4 GM-CSF/IFN-γ- and GM-CSF/IL-3/IFN-γ-deficient mice tested, demonstrated impaired phagocytosis of apoptotic cells, similar to GM-CSF- and GM-CSF/IL-3-deficient mice.

Surviving animals contained normal numbers of: B220, CD3, CD4, CD8, NK1.1, NK1.1-T, CD80, CD86, and CD11c positive cells. Gr-1 and Mac-1 positive cells, however, were increased twofold. The thymi of the GM-CSF/IFN-γ- and GM-CSF/IL-3/IFN-γ-deficient mice maintained normal T cell maturation (20 animals were analyzed by FACS®).

Over time, GM-CSF/IFN-γ- and GM-CSF/IL-3/IFN-γ-deficient mice gradually became moribund, with most requiring sacrifice by the age of 14 months (Figure 3.2.1 A). At autopsy, acute and chronic inflammatory reactions were present in many organs, particularly in the: lungs, soft tissues, lymph nodes, ovaries, adrenal glands, and liver (Figure 3.2.1 C). *Pasteurella pneumotropica* and enterococcal species were frequently cultured from these lesions (Figure 3.2.1 B) (8). Bone marrow myeloid hyperplasia and splenic extra-medullary hematopoiesis were associated with the persistent infections. In total, 39 out of 45 mice exhibited severe inflammatory lesions.

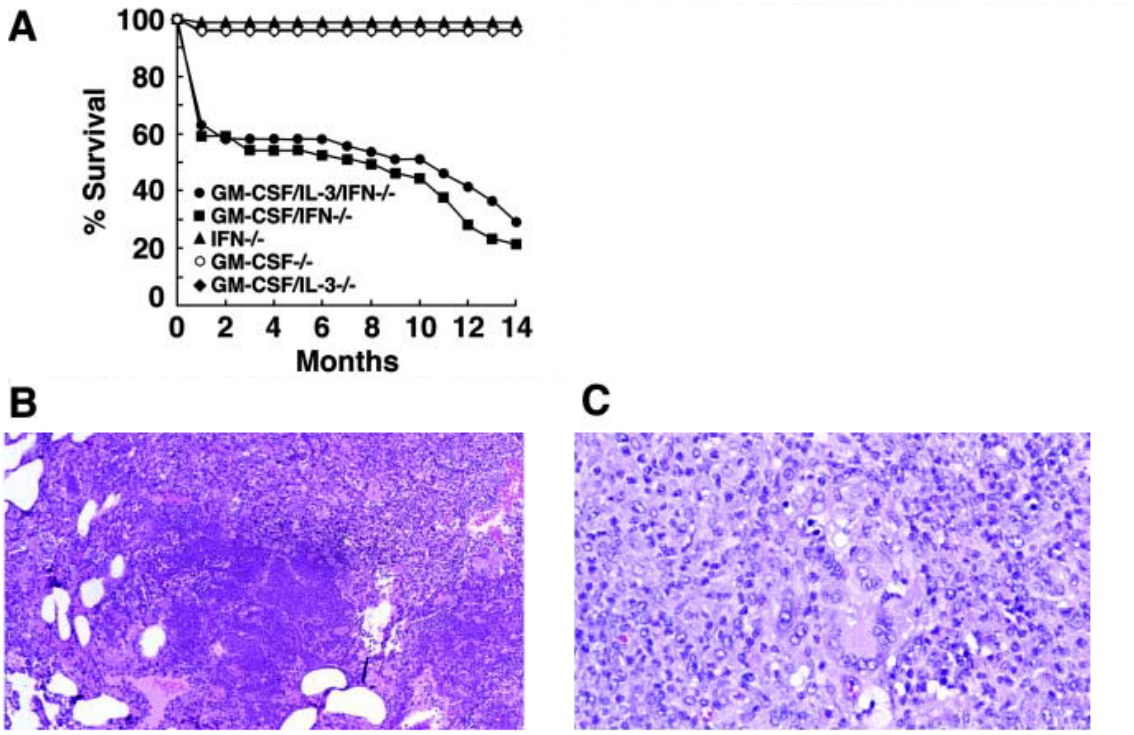

Figure 3.2.1 Reduced survival, infection and inflammation in GM-CSF/IFN-γ- and GM-CSF/IL-3/IFN-γ-deficient mice. (A) Survival curves for mice singly, or multiply, deficient in: GM-CSF, IL-3, and IFN-γ. The number of animals per cohort were: GM-CSF/IL-3/IFN-γ- (n = 29), GM-CSF/IFN-γ- (n = 44), IFN-γ- (n = 14), GM-CSF- (n = 18), GM-CSF/IL-3-deficient mice (n = 18). (B) This section shows a lethal bacterial pneumonia. The lung was infiltrated with numerous bacteria and neutrophils (H & E stain, original magnification x 200). (C) This section shows a granulomatous inflammation with multinucleated giant cells (H & E stain, original magnification x 400).

In contrast to the intense inflammatory responses, the SLE-like disorder was attenuated in GM-CSF/IFN-γ- and GM-CSF/IL-3/IFN-γ-deficient mice compared with GM-CSF- and GM-CSF/IL-3-deficient animals. Lymphoid aggregates were absent from the renal pelvis, and the immune-mediated glomerulonephritis was mild and resembled to

a nephritis. Moreover, anti-dsDNA autoantibodies, rheumatoid factors, and anti-C1q reactivity were markedly reduced (Figure 3.1.1 C and D) (8).

3.3 GM-CSF/IFN-γ- and GM-CSF/IL-3/IFN-γ-Deficient Mice Develop Cancer

Within the background of chronic infection and inflammation, a high proportion of the GM-CSF/IFN-γ- and GM-CSF/IL-3/IFN-γ-deficient mice developed lymphoproliferative diseases (Figure 3.3.1 A). Atypical lymphoid hyperplasias originating in mesenteric lymph nodes or Peyer's patches (141) frequently evolved to mature B cell lymphomas ($B220^+$, Ig^+ by immunohistochemistry) involving the liver, spleen, and other organs (36 out of 40 lymphomas examined were of B cell type) (Figure 3.3.1 B) (8). Pathologically, the tumors ranged from low-grade lesions with plasmacytoid features to high-grade diffuse large cell lymphomas with abundant mitoses (Figure 3.3.1 C and D) (8).

A

Pathology	GM-CSF/IFN-γ- (n=29)	GM-CSF/IL-3/IFN-γ- (n=16)
Atypical lymphoid hyperplasia	6	3
Lymphoma	16	12
Solid tumors	14	8

B

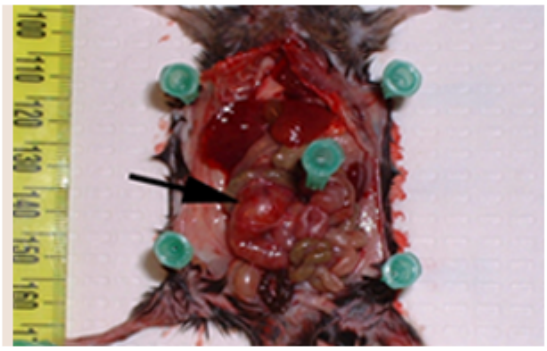

C

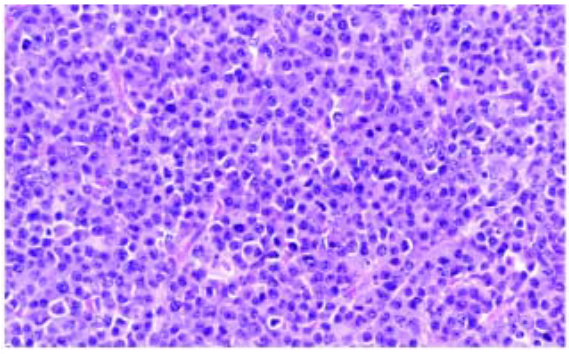

D

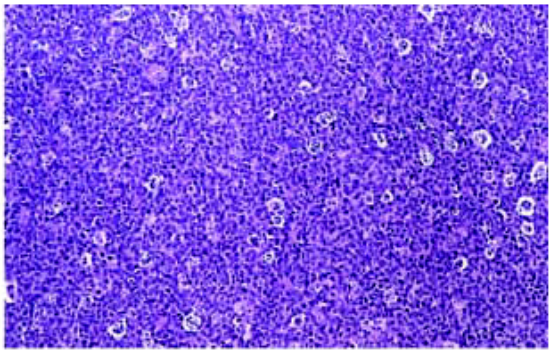

Figure 3.3.1 Tumors in GM-CSF/IFN-γ- and GM-CSF/IL-3/IFN-γ-deficient mice. (A) This table shows the spectrum and incidence of spontaneous tumors. (B) Typical location of a B cell lymphoma (arrow), originating in the mesenteric area. (C) Plasmacytoid lymphoma (H & E stain, original magnification x 400). (D) High grade diffuse large cell lymphoma with abundant mitoses ('starry sky' appearance) (H & E stain, original magnification x 400).

Southern analysis of immunoglobulin light and heavy chain gene rearrangements established that the proliferations were clonal (Figure 3.3.2 A and B). SKY analysis of metaphase spreads further disclosed chromosomal translocations and aneuploidy in 3 out of 6 tumors examined (Figure 3.3.2 C) (8). 3 out of 3 lymphomas tested were efficiently transplanted into young GM-CSF/IL-3/IFN-γ-deficient recipient mice.

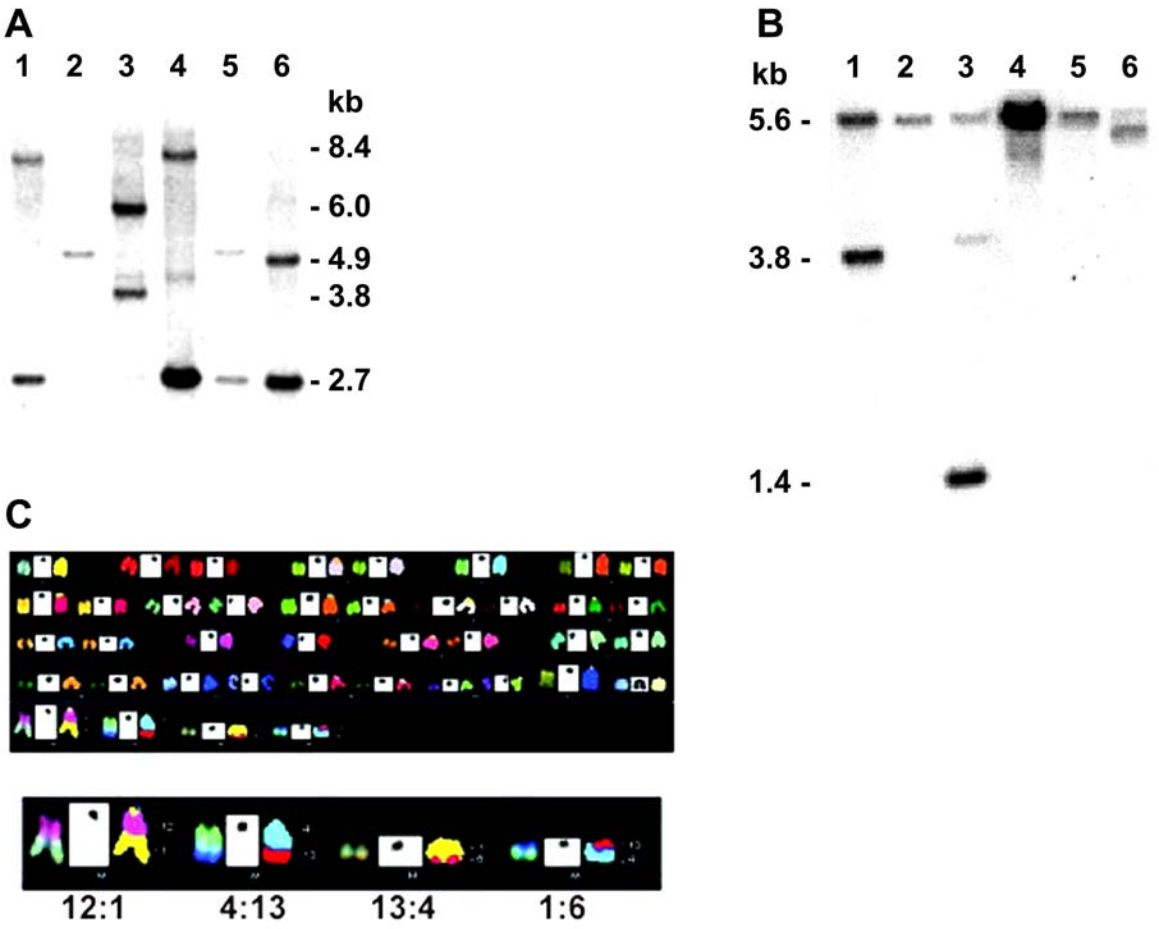

Figure 3.3.2 Tumor-derived DNA from 6 different B cell lymphomas was analyzed by Southern blots using: (A) an Jκ probe (germline band: 2.7 kb), and (B) a heavy chain probe (germline band: 5.6 kb). (C) Single cell lymphoma suspensions were stimulated with anti-CD40 antibodies (BD PharMingen), and SKY analysis of metaphase spreads were performed. Shown here are clonal: 12:1, 4:13, 13:4, and 1:6 chromosomal translocations.

In addition to the lymphomas, nearly 50% of the GM-CSF/IFN-γ- and GM-CSF/IL-3/IFN-γ-deficient mice developed solid tumors. The pathologies observed ranged from lesions that resembled well-described benign tumors in the human to carcinomas with metastases. Ovarian tumors were the most common, with 6 out of 29 doubly

deficient and 4 out of 16 triply deficient females manifesting: choriocarcinomas (Figure 3.3.3 A), luteomas, or teratomas. The broad spectrum of tumors also included: carcinomas of the biliary tract/liver (Figure 3.3.3 B), salivary glands, and bladder as well as adenomas/hyperplasias of the pancreatic islets, seminal vesicles, and osteochondral junctions. Moreover, 4 out of 29 doubly deficient and 4 out of 16 triply deficient animals showed multiple solid lesions.

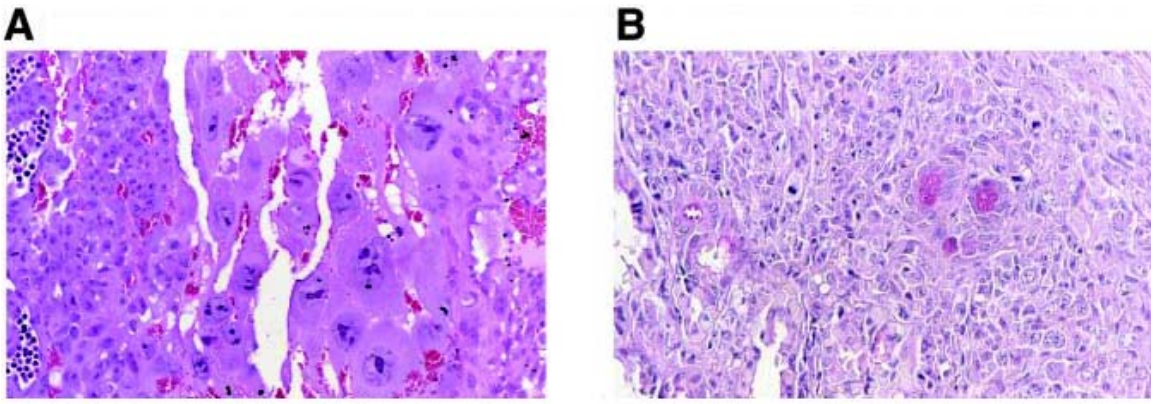

Figure 3.3.3 Solid tumors in GM-CSF/IFN-γ- and GM-CSG/IL-3/IFN-γ-deficient mice. (A) Choriocarcinoma (H & E stain, original magnification x 200). (B) Mucin-positive biliary tract/liver carcinoma (mucicarmine stain, original magnification x 400).

Tumor development required the combined deficiency of GM-CSF and IFN-γ. Histopathological analysis of other aged animals (12-17-months-old) revealed no tumors in 7 WT mice, only 2 cases of atypical hyperplasia and one benign luteoma in 20 GM-CSF-deficient mice, 2 cases of atypical hyperplasia in 17 GM-CSF/IL-3-deficient mice, and one luteoma and one islet cell hyperplasia in 13 IFN-γ-deficient mice. Moreover, gross autopsy of additional 28 IFN-γ-deficient mice, up to 27 months of age, disclosed only one single case of a $B220^{+}$ lymphoma.

3.4 Lymphomas Show Upregulation of the Pro-Inflammatory Protein COX-2

COX-2, the inducible form of the COX enzymes (142), catalyzes the synthesis of large amounts of prostaglandins with diversified biological activities, and its upregulation plays a vital role in: inflammation, tissue damage, and tumor development (143, 144). Total RNA from the tissues of 4 frozen $B220^+$ lymphomas was isolated and cDNAs were generated. As a control, I used total RNA from whole spleen of a WT C57Bl/6 mouse. Real Time PCR was performed using specific primers for COX-2. The relative amounts of COX-2 cDNAs were calculated by normalization of the threshold values of the COX-2 amplification plots to those of the amplification plots of the housekeeping gene cyclophilin. COX-2 turned out to be clearly upregulated in all 4 lymphomas tested compared to WT spleen (Figure 3.4.1 A). Moreover, histological staining of frozen sections using an HRP-labeled anti-COX-2 antibody (BD PharMingen) revealed a similar upregulation of COX-2 expression on the protein level, indicating that tumor cells themselves generated COX-2 (Figure 3.4.1 B).

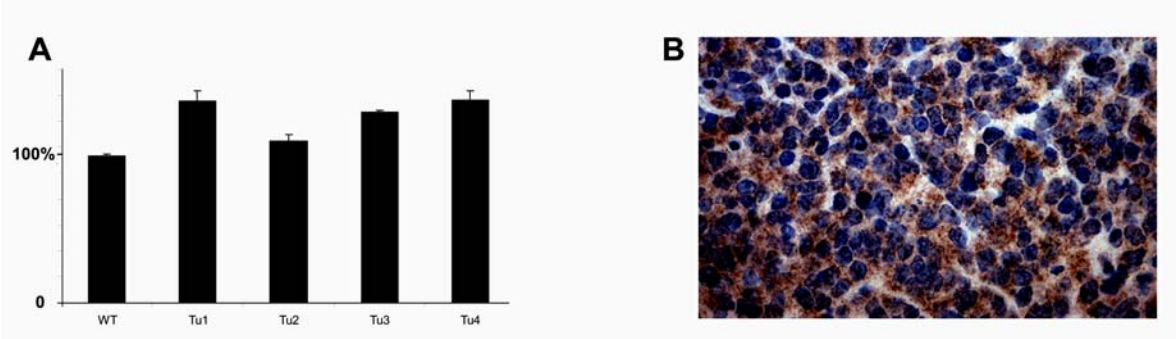

Figure 3.4.1 (A) COX-2 expression in 4 lymphomas (Tu 1-4), WT splenocytes as a control (all reactions were performed in triplicate, the WT splenic COX-2 expression was set as 100%). (B) Immunhistochemical analysis of COX-2 expression in $B220^+$ lymphoma cells using a HRP-labeled anti-COX-2 Ab (original magnification x 400).

3.5 Antibiotics and Anti-Inflammatory Agents (COX Inhibitors) Suppress Tumor Formation in GM-CSF/IFN-γ- and GM-CSF/IL-3/IFN-γ-Deficient Mice

As microbial agents, and unresolved inflammation, contribute to lymphomagenesis and cancer (145), I maintained cohorts of 12 female and male GM-CSF/IL-3/IFN-γ-deficient mice from birth on the antibiotic enrofloxacin or on the combined COX-1/COX-2 inhibitor sulindac. Consistent with the ability of enrofloxacin to suppress *Pasteurella pneumotropica* and enterococcal species (140), early infectious deaths were eliminated from mice treated with the antibiotic. Surprisingly, mice under the anti-inflammatory agent sulindac also survived the early lifespan (Figure 3.5.1). Moreover, both anti-microbial and anti-inflammatory treatment prevented tumor formation in the aged animals nearly completely. No lymphomas, or solid tumors, were detected in 19 mice of the enrofloxacin group autopsied at 14 months ($P < 0.001$ for lymphomas, $P < 0.001$ for all solid tumors, and $P = 0.03$ for carcinomas, determined by the Fisher exact test, compared with the untreated cohorts). One animal in the enrofloxacin group showed atypical thymic hyperplasia; 3 male mice died of fighting-related injuries, and 2 of unknown causes (between 8 and 14 months of age). Similar results were obtained in the cohorts treated with sulindac. In this group, 2 mice likely died from kidney failure caused by sulindac (as a known side-effect, this drug causes vasoconstriction of the small renal arteries (146)), and 2 mice died of unknown cause (between 8 and 14 months of age). Only one B cell lymphoma, but no solid tumor, could be found in one of these animals at autopsy conducted at 14 months of age ($P < 0.001$ for lymphomas, $P < 0.001$ for all solid tumors). The suppression of tumor formation in all the cohorts treated with enrofloxacin, or sulindac, was associated with a marked reduction in chronic inflammatory lesions; of 9 animals studied by histopathology, only one mouse showed a mild cholangitis.

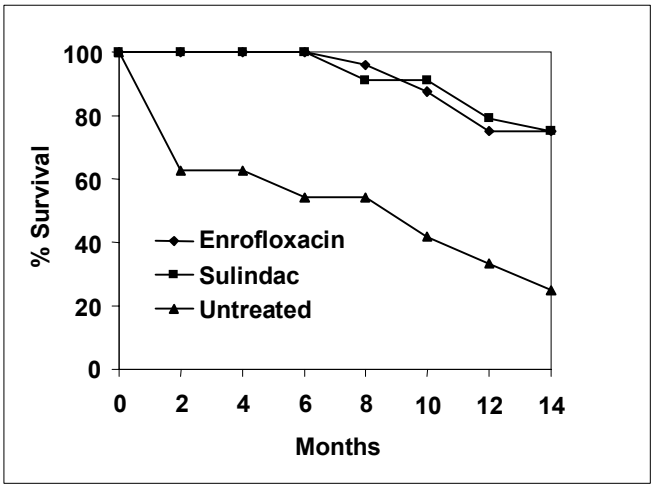

Figure 3.5.1 Survival curves for GM-CSF/IL-3/IFN-γ-deficient mice with and without anti-microbicidal or anti-inflammatory treatment. Cohorts of 12 female and 12 male GM-CSF/IL-3/IFN-γ-deficient mice (*n* = 24 mice per group) were treated with enrofloxacin or sulindac and compared to untreated triply cytokine-deficient controls.

3.6 Lymphomagenesis in GM-CSF/IFN-γ- and GM-CSF/IL-3/IFN-γ-Deficient Mice

To explore the mechanisms underlying spontaneous tumor formation in the compound cytokine deficient mice, I characterized potential precursor lesions in B cell lymphomagenesis. Although secondary lymphoid tissues of 2-3-months-old mice did not show evidence of atypical hyperplasia or clonal proliferation, their germinal centers (GCs) were enlarged. Consistent with these findings, serum IgG1 levels were higher in mutant mice than controls (1.811 ± 329, GM-CSF/IFN-γ-deficient versus 921 ± 172, WT; P = 0.0003); serum IgG2b (4,431 ± 2,150 versus 2,240 ± 730) and IgE levels (845 ± 709 versus 330 ± 427) were also increased, but these did not reach statistical significance (8).

To determine whether intrinsic B cell defects were involved, I evaluated the responses of purified B cells to stimulation with anti-CD40 antibody or LPS. No significant differences in the cell cycle profiles, or up-regulation of surface MHC II, CD80, CD86, fasR (CD95), or fasL (CD95L) expression, were detected between the mutant and WT B cells after 48 hours of stimulation. However, activated B cells from GM-CSF/IFN-γ- and GM-CSF/IL-3/IFN-γ-deficient mice manifested a resistance to fas-mediated apoptosis ($P < 0.0001$, versus WT), whereas activated B cells from IFN-γ-, GM-CSF-, or GM-CSF/IL-3-deficient animals displayed fas sensitivities equivalent to controls (Figure 3.6.1 A) (8). Nonetheless, apoptosis induced with: etoposide, staurosporine, and actinomycin, was comparable among all the strains.

In order to elaborate the cause underlying the fas resistance in the GM-CSF/IFN-γ- and GM-CSF/IL-3/IFN-γ-deficient mice, I determined in stimulated B cells by immunoblots the expression levels of the anti-apoptotic caspase-8 inhibitor FLIP (BD PharMingen), and the pro-apoptotic Death Associated Kinase (DAP Kinase; BD PharMingen) (147, 148). RNA levels of caspases: 1, 2, 3, 5, 6, 7, 8, 10, 11, 12, 13, and 14, FADD, FAP, FAF, TRAIL, TNFR, TRADD, RIP, bcl-x, bak, bax, bcl-2, and bad were checked by RNase protection assays. No significant differences in expression of all these proteins or RNAs between WT and GM-CSF/IL-3/IFN-γ-deficient B cells after 48 hours of stimulation could be found. Total NF-κB binding activity was determined by

EMSA using nuclear extracts and a canonical NF-κB binding sequence, but no differences between WT and GM-CSF/IL-3/IFN-γ-deficient B cells could be seen (3 mice tested per group).

As soluble factors modulate target cell fas sensitivity (149), I tested whether conditioned media from activated WT B cells could reverse the defective fas response of GM-CSF/IFN-γ- and GM-CSF/IL-3/IFN-γ-deficient B cells. As illustrated in Figure 3.6.1 B, the addition of WT supernatants to mutant cultures restored the fas sensitivity, suggesting that the impaired function of one or more cytokines might be responsible for the defect. Indeed, anti-TNF-α antibodies (BD PharMingen) significantly inhibited fas-mediated apoptosis in WT B cells, and supernatants from WT cultures contained 5 times more immunoreactive TNF-α (6.7 ± 0.44 pg/5 x 10^6 cells) than GM-CSF/IL-3/IFN-γ-deficient cell cultures (1.3 ± 0.21 pg/5 x 10^6 cells), as measured by TRFA-ELISA.

The restoration of normal TNF-α levels in the mutant cultures with the recombinant cytokine (BD PharMingen) partially corrected the fas resistance (Figure 3.6.1 B). Moreover, the restoration of WT TNF-α and IFN-γ levels (2.5 ± 0.06 pg/5 x 10^6 cells) completely restored the fas sensitivity of the mutant cells. These results establish a dual requirement for TNF-α and IFN-γ in fas-mediated B cell apoptosis. As aged fas-deficient mice harbor B cell lymphomas (150), this apoptotic defect, together with the phagocytic defect also seen in the GM-CSF/IFN-γ- and GM-CSF/IL-3/IFN-γ-deficient mice, may contribute to tumor development.

Despite lacking tumors, B cells of GM-CSF/IFN-γ- and GM-CSF/IL-3/IFN-γ-deficient mice, kept under enrofloxacin or sulindac, showed a similar resistance in fas-mediated apoptosis and phagocytic defects than untreated mice did.

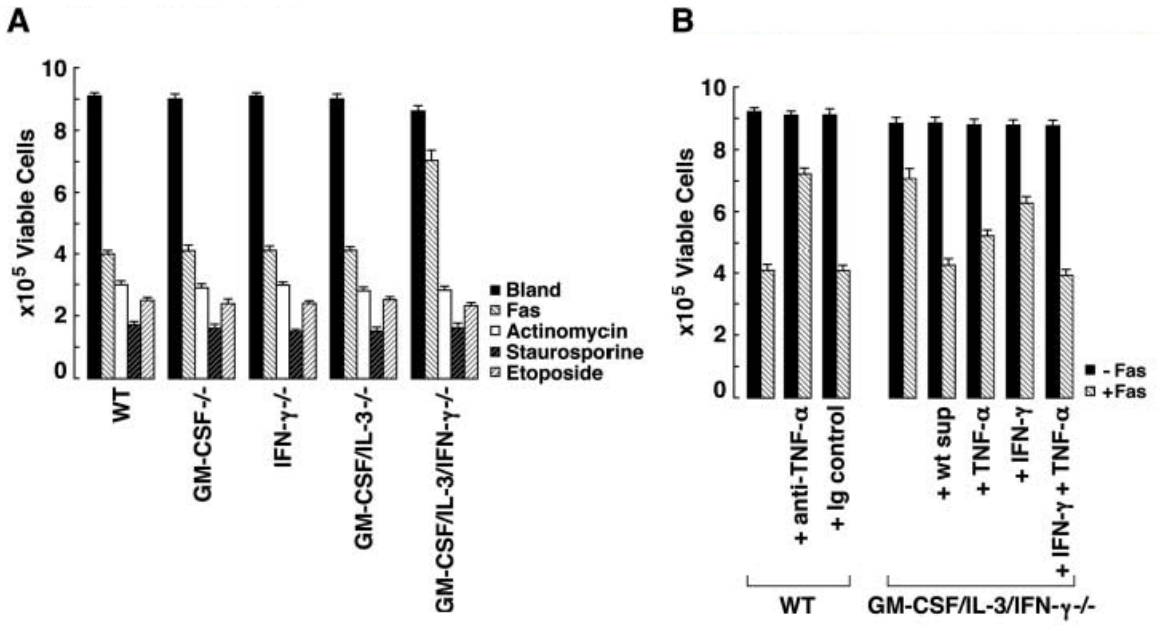

Figure 3.6.1 Impaired fas-mediated apoptosis. (A) Purified splenic B cells were stimulated for 48 hours with an anti-CD40 antibody. Then, 10^6 cell aliquots were incubated with 1 μg of anti-fas antibody, 100 μM etoposide, 1 μM staurosporine, or 2 μg/ml of actinomycin D for 12 hours and cell viability was determined by trypan blue exclusion. Data were pooled from 6 independent experiments; fas-treated WT versus fas-treated GM-CSF/IL-3/IFN-γ-deficient B cells ($P < 0.0001$). Similar results were obtained with LPS (50 μg) stimulated B cells. A comparable resistance to fas-mediated apoptosis was also found with GM-CSF/IFN-γ-deficient B cells. (B) TNF-α and IFN-γ were required for fas-mediated B cell apoptosis. The data were obtained from 4 independent experiments.